Epitaxy and controlled oxidation of Chromium ultrathin films on ferroelectric $BaTiO_3$ templates

Marco Asa[1], Christian Rinaldi[1], Luca Nessi[1], Daniela Petti[1], Edoardo Albisetti[1], Riccardo Bertacco[1], and Matteo Cantoni[1,a]

[1] *Dipartimento di Fisica, Politecnico di Milano, Via G. Colombo 81, 20131 Milano, Italy*

ABSTRACT

Interfaces play a crucial role in the study of novel phenomena emerging at heterostructures comprising metals and functional oxides. In this work, we consider $Cr/BaTiO_3$ heterostructures grown on $Nb:SrTiO_3$ (100) substrates. Chromium thin films with 2 nm nominal thickness are deposited by molecular beam epitaxy on the $BaTiO_3$ layer, and subsequently annealed in vacuum at temperatures ranging from 800 K to 970 K, and finally exposed to 30 L of molecular oxygen. Highly ordered films are obtained for each of this condition, ranging from metallic Cr to insulating Cr_2O_3 with tetragonal structure. Quite unexpectedly, an intermediate – fully ordered - case exist, whit the co-presence of Cr and Cr_2O_3 compounds, each one with its proper crystal orientation. These results show the opportunity of controlling the metal/oxide state of crystalline Cr films grown onto the ferroelectric template $BaTiO_3/Nb:SrTiO_3$.

[a] Author to whom correspondence should be addressed: matteo.cantoni@polimi.it

HIGHLIGHTS:

- Chromium films grown by MBE on BaTiO3/Nb:SrTiO3 are epitaxial up to 2 nanometers.
- Insulating Cr2O3 is obtained from Cr by activated migration of oxygen from BaTiO3.
- Crystalline Cr and Cr2O3 phases can coexist on BaTiO3/Nb:SrTiO3 templates.
- Nb doping of SrTiO3 substrates stabilizes a crystalline Cr film on a BaTiO3 layer.

KEYWORDS:

- A1. Crystal structure
- A1. Low dimensional structures
- A2. Single crystal growth
- A3. Molecular beam epitaxy
- B1. Oxides
- B1. Metals

1. INTRODUCTION

Interfacing metallic and oxide thin films is a key topic in the modern technology, because of the large variety of applications and technological challenges embedded in metal-oxide structures. In fact, the possibility of combining oxides with metallic layers is fundamental for microelectronics, but also to provide a testbed for new physical phenomena, arising from the combination of functional oxides and metals. Nevertheless, interfaces between reactive metals and oxides may become unstable, especially when exposed to thermal load, as diffusion of chemical species across the interface follows an Arrhenius type law. Such mechanism can be exploited for the formation of novel interfacial phases, such as transition metal oxides, which may exhibit novel and interesting properties [1, 2, 3].

In this work, we study the metal/oxide template Cr/$BaTiO_3$, with focus on the formation of oxides at the interface. Chromium is particularly suitable for this study, thanks to the high reactivity of the 3d metal as well as its relatively abundant on Earth and its antiferromagnetic properties [4]. Moreover, the Cr lattice makes it suitable for the epitaxial growth on both metals (e.g., Au [5], Ag [6], and Fe [7]) and oxides (e.g., MgO [8], $SrTiO_3$ [9], TiO_2 [10], and Al_2O_3 [11]). Oxides such as $SrTiO_3$ [9] and $BaTiO_3$ [12] can lead to the oxidation of Cr at the interface depending in the growth conditions. Among them, $BaTiO_3$ (BTO) is a prototypical ferroelectric oxide with perovskite structure, widely employed for different applications, from magneto-electric coupling with metals [13, 14, 15] and oxides [16], to electroresistive devices [17], even with memristive capabilities [18], to dedicated applications exploiting its piezoelectric, pyroelectric, and/or electro-optic properties [19]. The possibility to control the magnetic anisotropy of an antiferromagnetic Mn_2Au layer by reversing the ferroelectric polarization of BTO in $Mn_2Au/BaTiO_3$ interfaces has been predicted [20].

In Ref. [12] we demonstrated that deposition of ultrathin (1-2 nm) Cr films on $BaTiO_3$/undoped-$SrTiO_3$ does not support the growth of crystalline Cr and leads instead to a disordered metallic layer for annealing temperatures up to 573 K. At higher temperatures, Cr gets oxidized and forms an ordered tetragonal Cr_2O_3 structure with an antiferromagnetic ground state [21].

Here we show that the crystalline growth of Cr on BTO seed layers is possible by substituting the undoped STO substrate with a doped one. Crucial in this investigation, the oxidation of Cr thin film in Cr(1-2)/BTO(50) (thickness in nanometers) grown on Nb-doped SrTiO3 (001) substrates may be finely controlled through thermally activated migration of oxygen from the $BaTiO_3$ underlayer. The topmost film can go from metallic to fully oxidized, through an intermediate state in which both phases coexist; remarkably, crystal order is preserved in all cases.

2. METHODS

The growth of Cr/$BaTiO_3$ heterostructures was performed by Pulsed Laser Deposition (PLD) and Molecular Beam Epitaxy (MBE) in a cluster tool where both techniques are available *in-situ* [22] and endowed with several spectroscopic and diffraction characterization techniques.

$BaTiO_3$ (BTO) films of 40 nm were grown on commercial Nb-doped (0.5% wt.) $SrTiO_3$ (001) substrates by PLD with an oxygen pressure of 0.53 mbar, after an annealing at 973 K for 30 minutes. A quadrupled Q-Switched Nd:YAG laser (266 nm), providing pulses 7 ns long with a fluence of 5.6 J/cm^2, has been operated at a repetition frequency of 2 Hz to generate a plasma from a stoichiometric target. The substrate temperature was kept at 873 K during the deposition. The growth was followed by an annealing in 0.5 bar of oxygen at 873 K, according to a well-established growth recipe [23].

Chromium layers with 2 nm nominal thickness were deposited by MBE in ultra-high vacuum (UHV, pressure < 10^{-9} mbar), with the substrate at room temperature and a deposition rate of about 1 Å/min. The thickness was later confirmed by photoemission. We present the results of three Cr samples with a different post-growth treatment:

i. annealing in UHV at 800 K for 20 minutes (sample A);
ii. annealing in UHV at 970 K for 20 minutes (sample B);
iii. annealing in UHV at 970 K for 20 minutes followed by exposure to 30 L of molecular oxygen (sample C).

The chemical, electronic and structural properties have been investigated *in-situ* by X-ray Photoemission Spectroscopy (XPS), Ultraviolet Photoemission Spectroscopy (UPS), X-ray Photoemission Diffraction (XPD) and Low Energy Electron Diffraction (LEED). Photoelectrons were excited by standard Al-Kα X-ray or He-I ultraviolet sources and collected by a Hemispherical Energy Analyzer (HEA) Phoibos 150 (SPECS™), yielding an acceptance angle of ±2.5°, a field view of ~1.4 mm^2 and an energy resolution of 1.03 eV for XPS and 0.18 eV for UPS. The O 1s peak of BTO was used as reference at a binding energy (530.1 eV), instead of the C 1s which was absence in these samples. All the measurements were done at room temperature.

.

3. RESULTS

3.1. Chemical properties

Fig. 1(a) reports the XPS spectra at normal incidence of the Cr 2p core level for the samples A, B, and C. Fig. 1(b) instead shows the comparison of Cr2p spectra for A and C samples with the reference spectra of Cr and Cr_2O_3. The latter were measured on Cr films grown on $BaTiO_3/SrTiO_3$ without and with annealing at 773 K, respectively, following the recipe reported in Ref. [12].

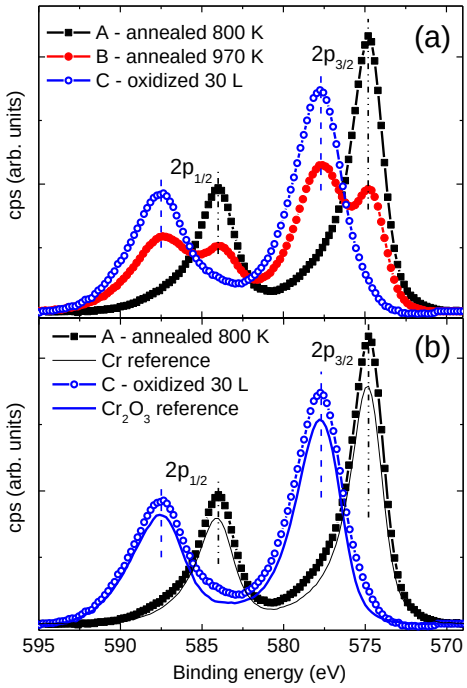

Figure 1: Cr 2p core level measured by XPS on Cr/$BaTiO_3$/Nb:$SrTiO_3$ (a) after different post-growth treatments (annealing at 800K and 970 K, additional exposure to 30L of oxygen), and (b) compared with Cr and Cr_2O_3 reference spectra.

Looking at Fig. 1(b) we can associate samples A and C to pure Cr and Cr_2O_3, respectively, given the binding energy of the core level as well as their line shape. On the other hand, sample B evidences the coexistence of two distinct oxidation states, the metallic (Cr^0) and an oxidized component (Cr^{3+}), of Cr 2p. The ratio between the corresponding areas, obtained by fitting the B line shape with the two reference components of Fig. 1(b), is $A_{Cr3+}/A_{Cr0} = 3.8 \pm 0.4$, pointing towards a preponderance of the oxidized component (about 80% of the total).

Thus, photoemission assets the stability of the metal/oxide interface up to 800 K, whereas the annealing at 970 K provides enough thermal energy to induce the partial oxidation of the Cr layer. Anyway, the annealing was not able to obtain the complete oxidation of the Cr film, despite the high temperature (970 K). The additional exposure to pure oxygen (30 Langmuir,

corresponding to 10^{-7} torr of molecular oxygen for 300 seconds in UHV environment) permits instead to achieve the complete oxidation of the overlayer. Note that the result is strongly affected by the substrate, since the almost complete oxidation was instead achieved when undoped $SrTiO_3$ substrate is used as substrate and already at lower temperature (770 K) [12]. This undoubtedly underlines that the substrate has a fundamental importance in determining the surface reactivity despite the intermediate layer of BTO.

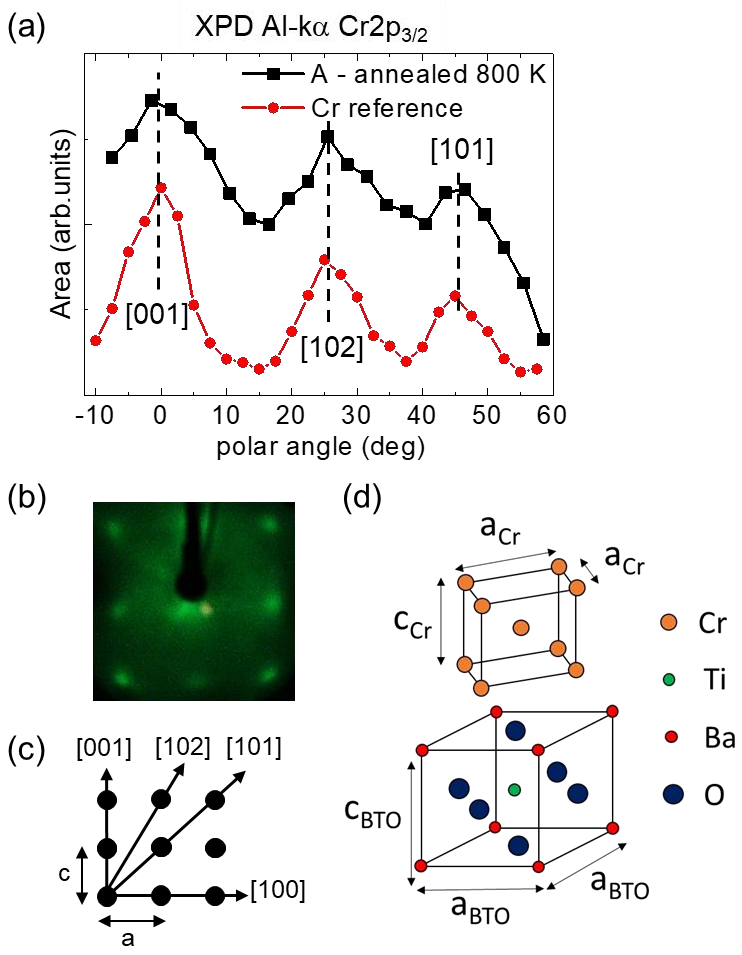

Figure 2: (a) XPD scans of the Cr $2p_{3/2}$ core level along the [110] $BaTiO_3$ azimuth of sample A (black squares) and a reference Cr film with [100] azimuth (red dots); (b) LEED diffraction pattern of sample A; (c) atomic sketch of the (010) plane of a tetragonal lattice, with indicated the crystal directions with larger atomic densities; (d) schematic arrangement of Cr and $BaTiO_3$ lattices, with a reciprocal rotation of 45°.

3.2. Structural properties

In Fig. 2(a) we report the photoelectron diffraction patterns (XPD) of the Cr 2p3/2 core level measured on sample A and on the reference single-crystal Cr film, for both along the BTO [110] azimuth [**Errore. Il segnalibro non è definito.**]. The crystalline quality of sample A is evident and compatible with that of the reference film, as confirmed by LEED pattern in Fig. 2(b). Looking at the nominal Cr and BTO lattice constants (a_{Cr}=0.2885 nm and a_{BTO}=0.3992 nm), an in-plane 45° rotation is expected to minimize the in-plane mismatch (2.2%, with respect to the 27.7% in case of cube-on-cube growth). As a matter of fact, the angular position of the diffraction peaks in Fig. 2(a) looks compatible with a cubic film with Cr [100] azimuth (Fig. 2(c)). The film orientation with respect to the underlayer is thus Cr[100]//BTO[110] and Cr[001]//BTO[001], as depicted in Fig. 2(d). The main diffraction directions in forward scattering regime, to which the peaks in Fig.2(a) are ascribed, are indicated. From the angular position of the [102] peak (25.5±0.5°), the ratio between out-of-plane and in-plane lattice parameters results larger than one (c/a=1.05±0.02), revealing a slight in-plane compression of the Cr cell. This can be ascribed to the in-plane lattice parameter of the BTO underlayer ($a_{BTO}/\sqrt{2}$=0.2822 nm, considering the 45° rotation) being smaller that the Cr one. Assuming that Cr grows with the same in-plane lattice parameter of the BTO underlayer and that the volume of the Cr unit cell is preserved, the c/a ratio would be indeed 1.07, coherent with our experimental findings. The observed c/a ratio is thus compatible with an unrelaxed (or slightly relaxed) Cr film, as can be reasonably expected considering the very small thickness (2±0.2 nm, from quartz microbalance and XPS analysis). We thus demonstrated that Cr thin films on BTO/STO annealed at 800 K are chemically and structurally equivalent to fully crystalline Cr films, apart from this small cell deformation.

On the opposite, completely oxidized Cr_2O_3 films can be obtained by exposure to a sufficiently high dose of oxygen, resulting in films similar to the ones obtained for Cr/$BaTiO_3$ annealed at 773 K on undoped $SrTiO_3$ (for further information, see Ref. [12]). XPD evidences a cubic structure (data not shown), with Cr_2O_3[100]//BTO[100] and Cr_2O_3[001]//BTO[001] thanks to the lattice-matching with the underlying $BaTiO_3$ layer (the Cr_2O_3 and BTO lattice constants are, respectively, a_{Cr2O3}=0.3990 nm [12] and a_{BTO}=0.3992 nm). In Ref. [12] we interpreted this result as the formation of a defective rocksalt structure, with 1 out of every 3 atoms of chromium missing in order to preserve the stoichiometry (Cr_2O_3).

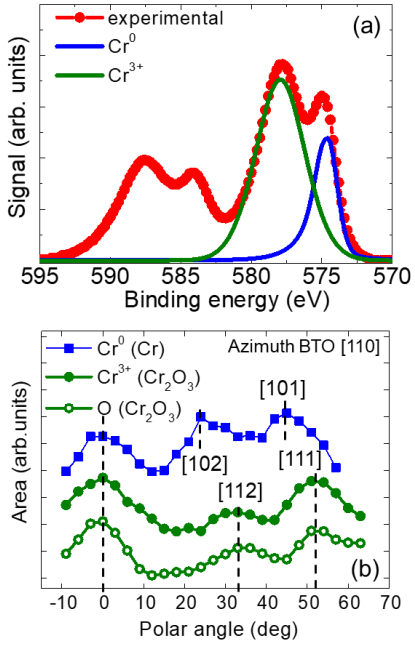

Figure 3: (a) Cr 2p core level measured by XPS on sample B (red dots). The 2p 3/2 component is deconvoluted into two components corresponding to Cr^{3+} (green thick line) and Cr^0 (blue thin line), with symmetrical (Voigt) and asymmetrical (Doniach Sunjic) lineshapes, respectively. (b) XPD of Cr^0 (blue squares), Cr^{3+} (green dots) and O1s (green empty dots) components along the [110] $BaTiO_3$ azimuth.

We now consider the intermediate situation obtained by the annealing at 970 K (sample B), leading to the coexistence of two Cr oxidation states (Cr^0 and Cr^{3+}) within the same thin film. In this case, the chemical sensitivity of the XPD is fully exploited, by evaluating the angular dependence of the peak intensity for the Cr^0 and Cr^{3+} components of the Cr $2p^{3/2}$ peak discussed in Fig. 1. The fit of the XPS spectra with two components, shown in Fig. 3(a) for the case of normal emission, was repeated for each polar angle. The O1s peak was acquired at the same angles. Figure 3(b) reports the resulting XPD patterns for Cr^0 (blue squares), Cr^{3+} (green full dots) and O1s (green empty dots) along the [110] BTO azimuth. Noteworthy, Cr^{3+} and O present the same structural orientation, as they pertain to Cr_2O_3. Instead, a different pattern is observed on Cr^0, associated to metallic Cr.

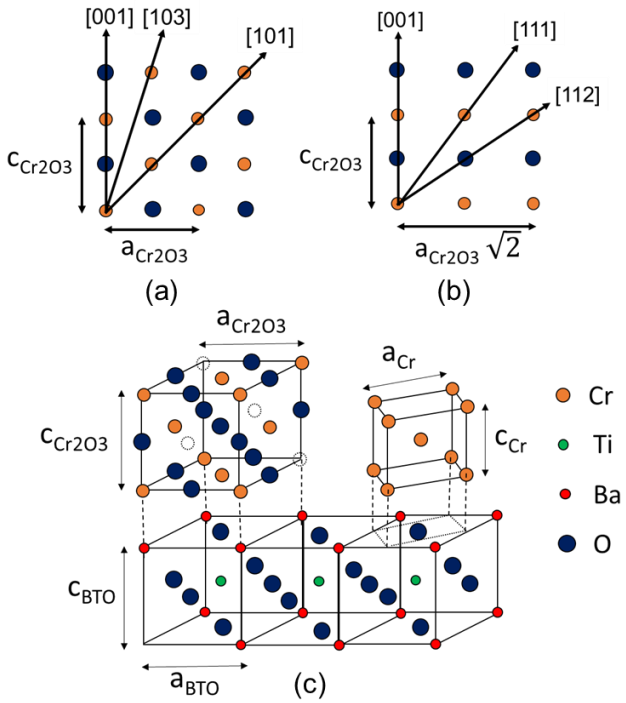

Figure 4: sketch of the atomic configuration of a rocksalt structure along the azimuths (a) [100] and (b) [110]; (c) schematic arrangement of Cr, Cr_2O_3 and BaTiO3 lattices.

In Fig. 4 is reported the sketch of the atomic configurations in a rocksalt structure along the azimuths [100] (panel a) and [110] (panel b). The crystal directions with the larger atomic densities are also indicated. Note that Cr_2O_3 crystallizes in a defective rocksalt structure, with one out of every three atoms of chromium missing in order to preserve the stoichiometry [12], even without influencing the position of the diffraction peaks.

Looking at the peaks in Fig. 3(b) in view of the atomic configurations in Fig. 4(a-b), it appears that, whereas the Cr^0 is again compatible with a tetragonal lattice with [100] azimuth (as in sample A), the [111] and [112] peaks of Cr3+ and O suggest a different situation, with the tetragonal lattice oriented along the [110] azimuth (as in sample C).

The picture arising from our results is the following: after the annealing of the Cr layer at 970 K, part of the Cr (about 80%, see Sect. 3.1) goes oxidized and crystallizes with the same orientation of the BTO underlayer (Cr_2O_3[110]//BTO[110]), whereas the remaining stays metallic and undergoes a 45° rotation (Cr[100]//BTO[110]). The minimization of the lattice mismatch is the driving force: the lattice constant of Cr_2O_3 is rather similar to that of BTO, allowing for the cube-on-cube growth (a_{Cr2O3}=0.399±0.003 nm [12] and a_{BTO}=0.3992 nm), whereas the lattice constant of Cr better fits with a 45° rotated BTO lattice (a_{Cr}=0.2885 nm and $a_{BTO}/\sqrt{2}$=0.2822 nm), as discussed above. In Fig. 4(c) we report, for simplicity, a schematic side-by-side arrangement of Cr and Cr_2O_3 regions on BTO to evidence the lattice relative orientations of the two regions with respect to BTO. However, a vertical arrangement, with e.g. Cr on top or Cr_2O_3 (the latter staying closer to BTO from which it takes the oxygen), cannot be excluded. Obviously, fine details of this mixed Cr/Cr_2O_3 arrangement (relative position and dimension of the two regions) cannot be accessed with this approach (a chemically-sensitive microscopic investigation, such as Auger microscopy and/or Electron Microscopy, would be needed), but are definitely beyond the scope of this paper.

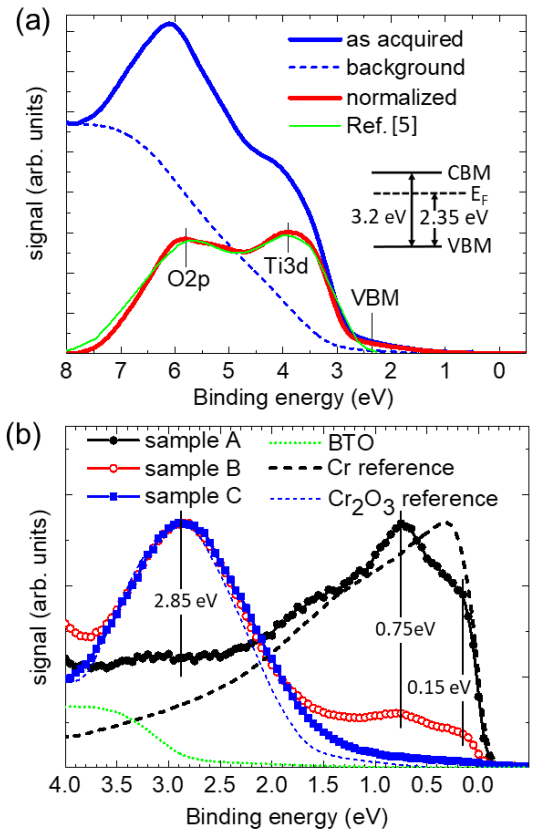

Figure 5: (a) BTO valence band, as acquired (blue) and after the normalization procedure (red), compared with a reference spectrum (green); (b) valence band of samples A (black dots), B (red empty dots), and C (blue squares), compared with reference spectra for BTO (green dotted line), pure Cr (black dashed thick line) and Cr_2O_3 (blue dashed thin line).

3.3. Valence band and metallic-insulator transition

The valence band (VB) of BTO and Cr/BTO samples A, B and C was investigated by UPS employing the He-I emission line (21.2 eV) to check the metallic or insulating properties of the Cr film. In Fig. 5(a) is reported the VB of BTO, prior to Cr deposition. The instrumental broadening (0.18 eV for UPS) can be neglected compared to the width of the structures in the spectra, so that the measured VB, normalized following the method reported in Ref. [24], can be identified with the density of states (DOS) of the BTO layer. The normalization consists in subtracting the inelastic background (blue dashed line) from the original data (blue line), and

correcting the result for the electron escape depth and the analyzer transmission function (both proportional, in first approximation, to KE^{-1}, where KE is the kinetic energy of photoelectrons). From a comparison between the obtained spectrum (red thick line) and Ref. [24] (green thin line), a valence band maximum (VBM) at 2.3±0.05 eV below the Fermi level can be inferred for our BTO film. In the inset, the energy arrangement of the valence band edges is reported, with the VBM, the conduction band minimum (CBM) and the Fermi level (E_F) indicated, considering a bandgap of 3.2 eV for bulk BTO at room temperature. Note that the two peaks at 3.9 eV and 5.8 eV (1.6 eV and 3.5 eV below the VBM), that can be ascribed to Ti 3d and O 2p electron states [25], are almost identical in the two spectra, confirming the bulk-like electronic structure of our BTO layer. However, above the VBM, a small but non-zero DOS appears. This can be ascribed to impurities or microscopic defects, such as oxygen vacancies acting as donors [26], introduced during the growth process. However, this behavior, coherent with the VBO shift mentioned above, is not expected to affect the ferroelectric properties of the $BaTiO_3$ film [23].

In Fig. 5(b) is reported the VB of Cr/BTO samples A (black dots), B (red empty dots), and C (blue squares), and the reference spectra for BTO (green dotted line), pure Cr (black dashed thick line) and Cr_2O_3 (blue dashed thin line). All data were normalized in the 0-9 eV energy range following the same method adopted for BTO [24]. The reference sample for pure Cr was the same employed in Sect. 3.1, whereas the Cr_2O_3 one was taken from Ref. [27]. Note that in all Cr/BTO samples any contribution from the BTO underlayer (blue dotted line) is negligible, as expected considering the reduced electron escape depth at such energies (about 1 nm [28]): as a matter of fact, where the VBM of BTO has a maximum, at 3.9 eV, all other samples present a minimum. Sample C and Cr_2O_3 reference fit quite well, with a single maximum at 2.85 eV in the investigated region (0-4 eV). Moving towards the Fermi level, sample C presents a smother decrease of the signal than Cr_2O_3, probably due to defects or isolated Cr atoms leading to a non-zero DOS.

In sample B, besides the peak at 2.85 eV two new features emerge: a maximum at 0.75 eV and a kink at 0.15 eV. Moreover, the signal is steeper around the Fermi level with respect to sample C, indicating a definitely larger DOS in this region. These observation are coherent with the scenery we suggested in Sect. 3.1: sample B is composed by insulating Cr_2O_3 (around 80%) and metallic Cr (around 20%), then features common to samples C (peak at 2.85 eV) and A (peak at 0.75 eV, kink at 0.15 eV, presence of a DOS at the Fermi level) coexist in the spectrum.

Sample A, finally, can be correlated to reference Cr, showing the same onset at the Fermi edge typical of a metal. The peak at 2.85 eV is absent (or negligible), pointing to the absence of Cr oxide. The peak shape is partially different, with a maximum at 0.75 eV and a kink at 0.15 eV in sample A, instead of a single peak at 0.3 eV in reference Cr. Note that the latter was prepared on undoped STO following the recipe in Ref. [12] leading to a non-crystalline structure, whereas, as we showed in Sect. 3.2, sample A is crystalline. Some difference between the DOS and band structures in the two cases, as we observe, is thus reasonably expected

4. CONCLUSIONS

We demonstrated the evolution of the Cr oxidation of Cr (2 nm) films on $BaTiO_3$ underlayers, grown by pulsed laser deposition on Nb-doped (0.5% wt.) SrTiO3 (001) substrates. Whereas annealing at 800 K produces ordered metallic Cr films, higher temperatures lead to the progressive formation of a tetragonal Cr_2O_3 phase, which coexists with the cubic metallic Cr. Both the phases are crystalline and minimize the mismatch with the substrate by following a different in-plane orientation (Cr[100]//BTO[110] vs. Cr_2O_3[110]//BTO[110]). Finally, an additional exposure to 30 L of molecular oxygen leads a fully oxidized film. Quite remarkably, crystal order is preserved anyway, whatever the oxidation degree is, allowing for the realization of metallic or insulating epitaxial Cr thin films on the same template, controlled by the post-growth conditions (annealing, oxidation).

ACKNOWLEDGEMENTS

This work was partially performed at Polifab, the micro and nanofabrication facility of Politecnico di Milano. This work was supported by PRIN project TWEET funded by MIUR (No. 2017YCTB59).

REFERENCES

[1] G. Radaelli et al., "Electric control of magnetism at the Fe/BaTiO3 interface", Nat.Comm. **5**, 3404 (2014). DOI: https://doi.org/10.1038/ncomms4404

[2] A. Paul et al., "Exotic exchange bias at epitaxial ferroelectric-ferromagnetic interfaces", Appl. Phys. Lett. **105**, 022409 (2014). DOI: 10.1063/1.4885316

[3] S. Hausmann et al., "Atomic-scale engineering of ferroelectric-ferromagnetic interfaces of epitaxial perovskite films for functional properties", Sci. Rep. **7**, 10734 (2017). DOI: 10.1038/s41598-017-10194-4

[4] E. Fawcett, "Spin-density-wave antiferromagnetism in Chromium", Rev. Mod. Phys. **60**, 209 (1988). DOI: 10.1103/RevModPhys.60.209

[5] M. C. Hanf, C. Pirri, J. C. Peruchetti, D. Bolmont, and G. Gewinner. "Formation of an interfacial alloy and epitaxial bcc Cr layers on Au(100)", Phys. Rev. B **39**, 1546 (1989). DOI: 10.1103/PhysRevB.39.1546

[6] C. Krembel, M. C. Hanf, J. C. Peruchetti, D. Bolmont, and G. Gewinner, "Growth of a flat Cr monolayer on Ag(100)", Phys. Rev.B **44**, 8407(R) (1991). DOI: 10.1103/PhysRevB.44.8407

[7] M. Riva, A. Picone, G. Bussetti, A. Brambilla, A. Calloni, G. Berti, L. Duò, F. Ciccacci and M. Finazzi, "Oxidation effects on ultrathin Ni and Cr films grown on Fe(001): A combined scanning tunneling microscopy and Auger electron spectroscopy study", Surf. Sci. **621**, 55 (2014). DOI: 10.1016/j.susc.2013.10.016

[8] M. A. Leroy et al., "Tunnel-mediated coupling between antiferromagnetic thin films", Phys. Rev. B **90**, 035432 (2014). DOI: 10.1103/PhysRevB.90.035432

[9] Q. Fu and T. Wagner, "Nucleation and growth of Cr clusters and films on (100) $SrTiO_3$ surfaces", Thin Solid Films **420**, 455 (2002). DOI: 10.1016/S0040-6090(02)00817-9

[10] Q. Fu and T. Wagner, "Metal/Oxide Interfacial Reactions: Oxidation of Metals on $SrTiO_3$ (100) and TiO_2 (110)", J. Phys. Chem. B **109**, 11697 (2005). DOI: 10.1021/jp050601i

[11] T. Wagner, Q. Fu, C. Winde, S. Tsukimoto, and F. Phillipp, "A Comparative Study of the Growth of Cr on (110)TiO_2 Rutile, (0001) α-Al_2O_3 and (100)$SrTiO_3$ Surfaces", Interface Sci. **12**, 117 (2004). DOI: 10.1023/B:INTS.0000012303.59127.37

[12] M. Asa, G. Vinai, J. L. Hart, C. Autieri, C. Rinaldi, P. Torelli, G. Panaccione, M. L. Taheri, S. Picozzi, and M. Cantoni, "Interdiffusion-driven synthesis of tetragonal chromium (III) oxide on BaTiO3", Phys. Rev. Materials 2, 033401 (2018). DOI: 10.1103/PhysRevMaterials.2.033401

[13] G. Radaelli et al., "Electric control of magnetism at the Fe/BaTiO3 interface", Nat.Comm. **5**, 3404 (2014). DOI: 10.1038/ncomms4404

[14] C.-G. Duan, S. S. Jaswal, and E. Y. Tsymbal, "Predicted Magnetoelectric Effect in Fe/$BaTiO_3$ Multilayers: Ferroelectric Control of Magnetism", Phys. Rev. Lett. **97**, 047201 (2006). DOI: 10.1103/PhysRevLett.97.047201

[15] M. Asa, L. Baldrati, C. Rinaldi, S. Bertoli, G. Radaelli, M. Cantoni, and R. Bertacco, "Electric field control of magnetic properties and electron transport in $BaTiO_3$-based multiferroic heterostructures", J. Phys.: Cond. Matt. **27**, 504004 (2015). DOI: 10.1088/0953-8984/27/50/504004

[16] W. Eerenstein, M. Wiora, J. L. Prieto, J. F. Scott and N. D. Matur, "Giant sharp and persistent converse magnetoelectric effects in multiferroic epitaxial heterostructures", Nat. Mat. **6**, 348 (2007). DOI: 10.1038/nmat1886

[17] G. Radaelli, D. Gutiérrez, F. Sanchéz, R. Bertacco, M. Stengel, and J. Fontcuberta, "Large room-temperature electroresistance in dual-modulated ferroelectric tunnel barriers", Adv. Mat. **24**, 2602 (2015). DOI: 10.1002/adma.201405117

[18] D. J. Kim, H. Lu, S. Ryu, C.-W. Bark, C.-B. Eom, E. Y. Tsymbal, and A. Gruverman, "Ferroelectric Tunnel Memristor", NanoLetters **12**, 5697 (2012). DOI: 10.1021/nl302912t

[19] A. K. Bain and P. Chand, *Ferroelectrics* (Wiley-VCH, 2017).

[20] E. Plekhanov, A. Stroppa, S. Picozzi, "Magneto-electric coupling in antiferromagnet/ferroelectric Mn2Au/BaTiO3 interface", Journal of Applied Physics 120, 074104 (2016). DOI: 10.1063/1.4961213

[21] M. Asa, C. Autieri, C. Barone, C. Mauro, S. Picozzi, S. Pagano, M. Cantoni, Detecting antiferromagnetism in tetragonal Cr2O3 by electrical measurements, Phys. Rev. B. 100 (2019) 174423. DOI: 10.1103/PhysRevB.100.174423.

[22] R. Bertacco, M. Cantoni, M. Riva, A. Tagliaferri, F. Ciccacci, "Epitaxial growth and characterization of layered magnetic nanostructures", Appl. Surf. Sci. **252**, 1754 (2005). DOI: 10.1016/j.apsusc.2005.03.123

[23] G. Radaelli, S. Brivio, I. Fina, R. Bertacco, "Correlation between growth dynamics and dielectric properties of epitaxial $BaTiO_3$ films", Appl. Phys. Lett. **100**, 102904 (2012). DOI: 10.1063/1.3692732

[24] R. Courths, “Valence band ups spectra and partial p and d density of states in SrTi03, BaTi03 and LiNb03” , Ferroelectrics, 26, 749 (1980). DOI: 10.1080/00150198008008163

[25] P. Pertosa, G. Hollinger, and F. M. Michel-Calendini, “Covalency effects in transition-metal perovskitelike compounds: Partial densities of p and d states and photoelectron valence-band spectra”, Phys. Rev. B 18, 5177 (1978). DOI: 10.1103/PhysRevB.18.5177

[26] Jong-Min Oh, Hyung-Jun Kim and Song-Min Nam, “Characterization of Leakage Current Mechanisms for Aerosol-deposited BaTiO3 Thin Films at Room Temperature”, Journal of the Korean Physical Society 57, 1096 (2010). DOI: 10.3938/jkps.57.1096

[27] F.L. Zimmermann, P. Steiner and S. Hufner, “Electron spectroscopies and partial excitation spectra in Cr_20_3”, Journal of Electron Spectroscopy and Related Phenomena 78, 49 (1996). DOI: 10.1016/S0368-2048(96)80024-7

[28] M. P. Seah and W. A. Dench, "Quantitative electron spectroscopy of surfaces: A standard data base for electron inelastic mean free paths in solids", Surface and Interface Analysis 1, 2 (1979). DOI: 10.1002/sia.740010103